Water Research 166 (2019) 115048

Contents lists available at ScienceDirect

Water Research

journal homepage: www.elsevier.com/locate/watres

Autochthonous dissolved organic matter potentially fuels methane ebullition from experimental lakes☆

Yongqiang Zhou [a, b, *], Lei Zhou [a, b], Yunlin Zhang [a, b], Javier Garcia de Souza [c], David C. Podgorski [d], Robert G.M. Spencer [e], Erik Jeppesen [f, g], Thomas A. Davidson [f, **]

[a] State Key Laboratory of Lake Science and Environment, Nanjing Institute of Geography and Limnology, Chinese Academy of Sciences, Nanjing, 210008, China
[b] University of Chinese Academy of Sciences, Beijing, 100049, China
[c] Instituto de Limnología 'Dr. Raúl A. Ringuelet' (ILPLA) (UNLP-CONICET), Boulevard 120 y 62, CC 712, La Plata, Provincia de Buenos Aires, Argentina
[d] Pontchartrain Institute for Environmental Sciences, Department of Chemistry, University of New Orleans, New Orleans, 70148, Louisiana, USA
[e] Department of Earth, Ocean and Atmospheric Science, Florida State University, Tallahassee, 32306, Florida, USA
[f] Department of Bioscience and Arctic Research Centre, Aarhus University, Vejlsøvej 25, DK-8600, Silkeborg, Denmark
[g] Sino-Danish Centre for Education and Research, Beijing, 100190, China

ARTICLE INFO

Article history:
Received 5 March 2019
Received in revised form
22 July 2019
Accepted 3 September 2019
Available online 5 September 2019

Keywords:
Methane (CH_4) ebullition
Chromophoric dissolved organic matter (CDOM)
Bio-labile
Parallel factor analysis (PARAFAC)
Ultrahigh resolution mass spectrometry
Greenhouse gases

ABSTRACT

Shallow lakes are hotspots for carbon processing and important natural sources of methane (CH_4) emission. Ebullitive CH_4 flux may constitute the overwhelming majority of total CH_4 flux, but the episodic nature of ebullition events makes determining both quantity and the controlling factors challenging. Here we used the world's longest running shallow-lake mesocosm facility, where the experimental treatments are low and high nutrients crossed with three temperatures, to investigate the quantity and drivers of CH_4 ebullition. The mean CH_4 ebullition flux in the high nutrient treatment (41.5 ± 52.3 mg CH_4–C m^{-2} d^{-1}) mesocosms was significantly larger than in the low nutrient treatment (3.6 ± 5.4 mg CH_4–C m^{-2} d^{-1}) mesocosms, varying with temperature scenarios. Over eight weeks from June to August covered here warming resulted in a weak, but insignificant enhancement of CH_4 ebullition. We found significant positive relationships between ebullition and chlorophyll-*a*, dissolved organic carbon (DOC), biodegradable DOC, δ^2H, $\delta^{18}O$ and $\delta^{13}C$-DOC, autochthonous dissolved organic matter (DOM) fluorescent components, and a fraction of lipids, proteins, and lignins revealed using ultrahigh-resolution mass spectrometry, and a negative relationship between ebullitive CH_4 flux and the percentage volume inhabited of macrophytes. A 24 h laboratory bio-incubation experiment performed at room temperature (20 ± 2 °C) in the dark further revealed a rapid depletion of algal-DOM concurrent with a massive increased CH_4 production, whereas soil-derived DOM had a limited effect on CH_4 production. We conclude that eutrophication likely induced the loss of macrophytes and increase in algal biomass, and the resultant accumulation algal derived bio-labile DOM potentially drives enhanced outgassing of ebullitive CH_4 from the shallow-lake mesocosms.

1. Introduction

Small shallow lakes are the most numerous lake type in the world and are hotspots of carbon processing and represent a large, yet poorly defined, source of atmospheric methane (CH_4) emission (Bogard et al., 2014; Holgerson and Raymond, 2016; Davidson et al., 2018). Lake ecosystems have been estimated to contribute 16%–24% of the world's CH_4 emission (Ciais et al., 2014; Saunois et al., 2016; Samad and Bertilsson, 2017) despite only covering <4% of the Earth's non-glaciated surface area (Verpoorter et al., 2015). Furthermore, approximately 50% of the world's lakes measured by

☆ This manuscript has not been published or accepted elsewhere. We have not submitted it to any other journals. The manuscript is organized according to the format and structure of your journal.

* Corresponding author. State Key Laboratory of Lake Science and Environment, Nanjing Institute of Geography and Limnology, Chinese Academy of Sciences, Nanjing, 210008, China.
** Corresponding author.
E-mail addresses: yqzhou@niglas.ac.cn (Y. Zhou), thd@bios.au.dk (T.A. Davidson).

https://doi.org/10.1016/j.watres.2019.115048
0043-1354/

surface area are located in climate-sensitive regions and the CH_4 emission from these small lakes has been estimated to be equivalent to roughly 60% of the emission from all natural CH_4 sources (Wik et al., 2016). Recent studies have revealed that nutrient enrichment and warming can interact to control the outgassing of CH_4, in particular fueling the ebullition of CH_4 (DelSontro et al. 2016, 2018a; Davidson et al., 2018). Both eutrophication and warming can fuel algal blooms leading to the loss of submerged macrophytes, and this potentially leads to enhanced diffusive and ebullitive CH_4 emissions, while submerged plants have been shown to be a potential sink of CH_4 (Davidson et al. 2015, 2018). Furthermore, increased algal biomass can result in an elevated production and accumulation of autochthonous dissolved organic matter (DOM) (Zhou et al., 2015), and this portion of algal-DOM may impact CH_4 production rates (West et al. 2012, 2015). Although a recent study have revealed that overall trophic status and macrophyte coverage greatly impact CH_4 ebullition from shallow-lake mesocosms (Davidson et al., 2018), the relative importance of autochthonous and allochthonous DOM, i.e. the carbon substrates on CH_4 ebullition, as well as the mechanisms underlying DOM and ebullitive CH_4 remain largely unknown. Archaeal methanogenesis has long been thought to be the major source of biogenic CH_4 (Thauer et al., 2008), and the effects of chlorophyll-*a* (Chl-*a*), a surrogate of algal biomass, and bulk dissolved organic carbon (DOC) on CH_4 production have been investigated (West et al., 2012; DelSontro et al., 2018b). A recent study have revealed that eutrophication overrode climate warming in enhancing the Chl-*a* levels and thereby the accumulation of autochthonous DOM (Zhou et al., 2018a), the linkage between this DOM fraction and CH_4 ebullition is, however, largely unknown. The chemical reactivity and biolability of DOM have long been considered to be largely determined by its source and chemical composition (Stedmon et al., 2007; Kowalczuk et al., 2013; Fu et al., 2016; Yang et al., 2017). To what extent there is a direct linkage between ebullition of CH_4 from shallow lakes and DOM composition is largely unknown. The CH_4 flux can be divided into three pathways: diffusive, plant-mediated and ebullitive flux, and in shallow and eutrophic lakes the ebullitive flux can contribute up to 95% of the total CH_4 emission (Davidson et al., 2018). The CH_4 ebullition generally increases with increasing primary productivity (DelSontro et al., 2016), but is highly stochastic (Bastviken et al., 2004), making estimation of the flux a challenging task (Wik et al., 2013). Microbes, especially archaea, fuel the rapid degradation of bio-labile DOM, and can result in oxygen depletion in the water column or lake sediment (Zhou et al. 2015, 2018b; Tang et al., 2017) and thereby a further increase in the ebullitive flux (Borges et al., 2015; DelSontro et al., 2016; Davidson et al., 2018).

DOM serves as carbon source for CH_4 emission in lake ecosystems and is comprised of a mixture of degradation by-products and freshly produced compounds that vary remarkably in molecular weight (Coble, 2007). Optical measurements including fluorescence coupled with parallel factor analysis (PARAFAC) have been utilised to trace the sources and composition of DOM in various aquatic ecosystems (Murphy et al., 2008; Hood et al., 2009; Yao et al., 2011; Guo et al., 2014; Hur et al., 2014; He and Hur, 2015). Recent studies have applied electrospray ionization Fourier transform ion cyclotron resonance mass spectroscopy (FT-ICR MS) to facilitate the characterisation of DOM in various aquatic ecosystems (Dittmar and Paeng, 2009; Stubbins et al., 2010; Spencer et al., 2014; Hawkes et al., 2016). The ultrahigh resolving power and mass measurement accuracy of FT-ICR MS allow the assignment of molecular formulae to thousands of DOM molecules and give considerable advances in obtaining compositional information (Mopper et al., 2007). In productive ecosystems, DOM derived from the degradation of aquatic organisms contributes importantly to the carbon pool and represents a considerable fraction of the bio-labile DOM (Hur et al., 2009; Zhang et al., 2009; Zhou et al., 2015; Huang et al., 2018; Song et al., 2018). Microbial cycling of bio-labile DOM may potentially fuel the outgassing of CH_4 (Zhou et al., 2018b). To date, however, to the best of our knowledge, there has been no attempt to characterise the direct linkage between DOM composition and bio-lability and the ebullition of CH_4. We combined investigation at a long-running mesocosm experiment mimicking shallow lakes with laboratory bio-incubation experiments to investigate the impact of DOM composition and bioavailability on the ebullition of CH_4. Ebullition was measured continuously, and the percentage volume inhabited (PVI) of submerged macrophytes and values of Chl-*a*, DOC and optical DOM were determined weekly to trace possible drivers of CH_4 ebullition. We hypothesised that highly bio-labile autochthonous DOM accumulated in the high nutrient mesocosms may fuel the outgassing of CH_4.

2. Materials and methods

2.1. Experimental setup

The experimental facility mimicking shallow lakes located in Lemming, Denmark (56.23°N, 9.52°E), has run continuously since August 2003 and is the longest running mesocosm experiment in the world aiming to unravel the combined effects of global warming and eutrophication on shallow lakes (Liboriussen et al., 2005). Briefly, the experiment consists of 24 fully mixed, flow-through experimental shallow-lake mesocosms (diameter = 1.9 m, water depth = 1 m, water residence time = 2.5 months) under six different treatments: three temperature levels crossed with two nutrient treatments (in four replicates). The three temperature treatments include unheated ambient mesocosms (AMB), IPCC climate scenario A2 (A2) (Houghton et al., 2001) and A2+ 50% (A2+) with temperatures 2–3 °C and 4–5 °C higher than AMB, respectively, depending on season (adjusted monthly). The monthly temperatures were determined from regional downscaling of the GCM models (Liboriussen et al., 2005) using 1960–1990 as the reference period and the modeled temperatures for 2071–2100 (Liboriussen et al., 2005). The A2 and A2+ mesocosms all exhibited seasonal and diurnal water temperature fluctuations following the AMB mesocosms (Liboriussen et al., 2005). Sediment collected from several natural lakes around Lemming, Denmark, was homogenised and added to the mesocosms (~10 cm depth) prior to the initialisation of the experiment in 2003, and all the mesocosms share identical initial conditions (Liboriussen et al., 2005). The experimental shallow-lake mesocosms are all fed by groundwater (dissolved inorganic carbon = 31.4 ± 3.8 mg L^{-1} and dissolved organic carbon (DOC) = 1.06 ± 0.42 mg L^{-1}), thus representing groundwater-fed small shallow lakes. The low nutrient experimental mesocosms receive no additional nutrients and total nitrogen (TN) and total phosphorus (TP) concentrations were 0.18 mg L^{-1} and 14 μg L^{-1}, respectively, during the experiment. The extra loading of TN and TP to the high nutrient experimental mesocosms are 7 mgN m^{-2} d^{-1} and 27.1 μgP m^{-2} d^{-1}, respectively. Within the mesocosms mean values of 3.17 mg L^{-1} TN and 417 μg L^{-1} TP during the experiment were observed for the high nutrient treatment. The extra nutrient loading caused a shift from the clear water conditions existing in the low nutrient mesocosms to turbid water in the high nutrient mesocosms.

There were no floating or emergent plants in the mesocosms, and we quantified the submerged plants as PVI in the water column following the approach detailed in reference (Davidson et al., 2018). Briefly, the coverage percentage and height of the submerged plants were determined, and the proportion of the mesocosms covered by submerged plants was correspondingly assessed. Plant

abundance was investigated weekly when gas and DOM samples were collected.

2.2. Ebullitive CH_4 sampling and flux calculations

The ebullitive flux was determined following the approach detailed in reference (Davidson et al., 2018). Briefly, specially designed gas traps with two inverted funnels connected with 500 mL glass bottles were placed right below the water surface in each mesocosm. The funnels were located ~0.2 m below the water surface in the same position in each mesocosm. The funnels cover an area of 0.0225 m^2 and represent ~0.8% of the total area of the mesocosms. This is a much larger proportion of the total mesocosm area compared with samples taken in typical natural lakes and the obtained ebullitive flux measurements are thus supposedly more reliable (Wik et al., 2013; Davidson et al., 2018). Samples were collected every week from June to August 2016 (8 occasions in total). The sample volume was determined and the CH_4 gas was collected from the bottle with a syringe (50 mL) fitted with a three-way stopcock using a specially designed lid equipped with rubber septa. The funnels and bottles were cleaned or replaced every week during the experiment. The volume of ebullitive bubbles never exceeded 400 mL during the experiment. Methane concentrations were determined on an Innova photoaccoustic gas monitor, which is suited to the very high concentrations of CH_4 (up to 100,000 ppm) in the bubbles. The results were validated using the results measured on an Agilent 7890 Gas Chromatograph system (Agilent, Denmark) (Davidson et al., 2018).

The ebullitive CH_4 flux was calculated using the method detailed in reference (Davidson et al., 2018):

$$\text{Ebullitive } CH_4 \text{ flux} = pCH4_{bub} \times Vol_{bub}/(t \times A) \quad (1)$$

where $pCH4_{bub}$ and Vol_{bub} are the CH_4 concentration and volume of the trapped bubbles, respectively. t and A are the sampling time interval and the area of the funnel (0.0225 m^2). Due to the very low solubility of CH_4, we assume the effect of re-dissolved CH_4 during the weekly sampling intervals to be minor (Davidson et al., 2018).

2.3. CDOM sample collection and bio-incubation experiment

Water samples were collected twice per day (at 19:00 and 07:00 the next morning) once a week for eight weeks from June to August 2016 from the experimental mesocosms using acid-cleaned Niskin bottles. A total of 387 water samples (24 mesocosms × 2 times per day × 8 weeks +3 source water (groundwater) samples) were collected and immediately filtered through Whatman GF/F filters (0.7 μm) and pre-rinsed Millipore membrane cellulose filters (0.22 μm) after which they were put on ice and stored in the dark while in the field.

DOC bio-lability is the degree to which DOC is available for microbial uptake, and operationally, biodegradable DOC (BDOC) is defined as the percentage of DOC being mineralized over a certain period of time, typically 28 days (Holmes et al., 2008; Mann et al., 2012; Abbott et al., 2014; Vonk et al., 2015). BDOC usually increased logarithmically with increasing incubation time and varies minimally after two weeks of bio-incubation (Spencer et al., 2015). DOM samples collected in the sixth week of the mesocosm experiment were used for 28 days of bio-incubation under room termperature (20 ± 2 °C) to unveil the bio-lability of DOC in the mesocosms and how BDOC may influence CH_4 ebullition following the methods detailed in Zhou et al. (2018a), and can be found in the Supporting Information.

To unravel the potential role of autochthonous algal-DOM in fuelling the outgassing of CH_4, we carried out a 24 h bio-incubation experiment for soil-DOM and algal-DOM. Soil-DOM and algal-DOM samples were used to simulate the optical properties of DOM samples collected from the groundwater-fed experimental facilities without and with the addition of external nutrients boosting algal blooms. Approximately 10 kg organic-rich topsoil from the Lake Taihu watershed and 10 L algae samples (enriched using phytoplankton net) from Lake Taihu were collected in the nearshore of Meiliang Bay, Lake Taihu, on 20 September 2018 during a *Microcystis* algal bloom. Approximately 20 L Mill-Q water was added to the topsoil and the algae samples, respectively. The mixtures were both shaken at 300 rpm for 30 min and then gently shaken several times a day to keep them oxidised and degraded in the dark at 20 ± 2 °C for three days. Soil-leachate and algal-water mixture were successively filtered through pre-rinsed Whatman GF/D (2.7 μm porosity) and Millipore filters (0.22 μm). The soil-DOM and algal-DOM samples were both diluted to ensure a roughly similar initial DOC concentration (~15 mg L^{-1}).

Three aliquots filtered through Millipore filters for both soil-DOM and algal-DOM determination were immediately (0 h) measured for CDOM absorption and fluorescence as well as DOC concentrations. Three additional aliquot filtrates for both soil-DOM and algal-DOM measurement were poured into 61 mL acid-cleaned and pre-rinsed brown glass bottles with excess DOM sample overflowing the bottles. The bottles were then immediately capped without headspace using a butyl rubber stopper and sealed with an aluminium cap. N_2 gas (ultrahigh purity, 99.999%) was injected into the bottle via two syringes to create a 10 mL headspace following the methods detailed in Xiao et al. (2017). Each vial for bio-incubation had the headspace flushed three times with N_2 gas for 30 s prior to the incubation. The bottles were shaken vigorously for 10 min to allow the dissolved CH_4 to get into equilibrium with the headspace. An approximately 5 mL gas sample was drawn from the headspace using a syringe with a three-way stopcork and injected into a gas chromatograph (Model Agilent GC6890N, Agilent Co., CA, USA) with a flame ionization detector for CH_4 detection. 2 mL soil- and algal-leachates filtered through GF/D filters (2.7 μm porosity) were used as bacterial inoculum, and extra nutrients were added following the aforementioned methods for BDOC measurements (Abbott et al., 2014; Vonk et al., 2015). After 24 h incubation (20 ± 2 °C), the samples were immediately filtered through Millipore filters for DOC, CDOM absorption and fluorescence measurements and headspace bottles filled with soil-DOM and algal-DOM samples were immediately measured for dissolved CH_4.

2.4. CDOM optical measurements, calibration and PARAFAC modelling

Details about CDOM absorption and fluorescence measurements, and the corresponding calibrations and PARAFAC modelling can be found in the Supporting Information. Using split-half validation analysis, random initialisation analysis and analysis of residuals (Stedmon and Bro, 2008; Murphy et al., 2013), we found that a six-component model was well-validated (Fig. S1; Fig. S2) (Zhou et al., 2018a).

2.5. DOC, chlorophyll-a (Chl-a), and stable isotopic $\delta^{13}C$-DOC, $\delta^{2}H$ and $\delta^{18}O$ measurements

Filtrates obtained via filtration through Whatman GF/F filters (24 mesocosms × 2 times per day × 8 weeks +3 source water (groundwater)) were measured for DOC using the NPOC method on a TOC-V CPN (Shimadzu, Tokyo, Japan) analyzer via combustion at ~680 °C. Chlorophyll-*a* (Chl-*a*) concentrations (24 mesocosms × 1 time per week × 8 weeks) were determined spectrophotometrically at 665 and 750 nm after extraction with ethanol by

centrifuging (3000 g for 10 min).

δ^{13}C-DOC can be used to trace the sources of DOC as δ^{13}C-DOC for terrestrial DOM typically ranges from −29‰ to −26‰ and autochthonous DOM typically from −25‰ to −20‰ (Hood et al., 2009; Spencer et al., 2014), and see details in the Supporting Information.

Evaporation fuels the enrichment of δ^{2}H and δ^{18}O in surface waters (Yamamoto-Kawai, 2005) and can therefore be used to reveal the source of water and ongoing environmental changes (Yamamoto-Kawai, 2005; Stedmon et al., 2015). Samples for determination of δ^{2}H and δ^{18}O were collected at 5 cm depth and analysed on an LGR DLT-100 (model: 908-0008) Laser Adsorption Spectroscope (Los Gatos Research, Inc., Mountain View, CA, USA). δ^{2}H and δ^{18}O were calibrated against Vienna Standard Mean Ocean Water (VSMOW). δ^{2}H and δ^{18}O had a precision of ±1.2‰ and ±0.3‰, respectively.

2.6. Fourier transform ion cyclotron resonance mass spectrometry (FT-ICR MS) analyses and data processing

Filtrates (n = 6) of each treatments (three temperature crossed with two nutrient levels) were solid phase extracted applying PPL Bond Elut (Agilent) resins prior to electrospray ionization in negative ion mode following the approach detailed in Spencer et al. (2014) and Dittmar et al. (2008) and in the Supporting Information. van Krevelen diagrams displaying atomic ratios of H/C vs. O/C can be used to unravel the composition of DOM molecules in various ecosystems (Kim et al., 2003; Stubbins et al., 2010; Ohno et al., 2014; Spencer et al., 2014; Kellerman et al., 2015). We classified the molecular formulas following the approach recommended by Ohno et al. (Ohno et al., 2014): (i) lipids (O/C = 0–0.3, H/C = 1.5–2.0), (ii) amino acids associated with proteins (O/C = 0.3–0.67, H/C = 1.5–2.2), (iii) lignins (O/C = 0.1–0.67, H/C = 0.7–1.5), (iv) carbohydrates (O/C = 0.67–1.2, H/C = 1.5–2.2), (v) unsaturated hydrocarbons (O/C = 0–0.1, H/C = 0.7–1.5), (vi) condensed aromatics (O/C = 0–0.67, H/C = 0.2–0.7), and (vii) tannins (O/C = 0.67–1.2, H/C = 0.5–1.5) (Ohno et al., 2014). The aliphatic peaks are categorised as having double bond equivalents (DBEs) per carbon atom <0.3 and ≥1 H/C ratio (Stubbins et al., 2010). Spearman rank correlation coefficients were determined between the relative abundance of the formulas assigned and CH_4 ebullition from the corresponding mesocosms (three temperature crossed with two nutrient levels).

2.7. Statistical analyses

Boxplot, linear, and nonlinear fittings were conducted using MATLAB R2015b software. Mean values, standard deviations (S.D.), *t*-test and ANOVA were performed with R i386 3.5.1. *t*-test, ANOVA and regression results with $p < 0.05$ were reported as significant. The relative importance of individual variables, including the PVI of macrophytes, Chl-*a*, DOC, and CDOM optical properties to the ebullition of CH_4, i.e. the percentage of variation explained, was determined using a *calc.relimp* function based on generalized linear model (GLM) inbuilt in R i386 3.5.1. Principal component analysis (PCA) of the samples collected from each individual mesocosm during the eight-week experiment was performed to determine the PVI of macrophytes, Chl-*a*, log(CH_4), DOC and DOM optical properties using the inbuilt statistics toolbox in MATLAB 2015b.

3. Results

3.1. PARAFAC modelling results

PARAFAC is an alternating least-squares algorithm that statistically decomposes DOM excitation-emission matrices (EEMs) of complex mixtures into a series of trilinear components, and the approach can be used to qualitatively trace the variability of DOM fraction in various ecosystems (Stedmon et al., 2003; Murphy et al., 2013). The six-component PARAFAC model explained >99.9% of the total signal of the EEMs dataset. We applied Openfluor (Murphy et al., 2014) – an online CDOM fluorescence library – to compare the spectral characteristics of the six components (Fig. S1; Fig. S2) with those identified earlier in other aquatic ecosystems. C1 (Ex: ≤ 230 and 340 nm/Em: 460 nm) can be categorised as a typical terrestrial humic-like fluorophore (Kowalczuk et al., 2009; Murphy et al., 2011; Kothawala et al., 2014; Shutova et al., 2014). C2 had spectral shapes (245/412 nm) similar to those of a fulvic-like fluorophores (Stedmon and Markager, 2005a; Murphy et al., 2011). C3 exhibited two Ex maxima (at 240 and 300 nm) corresponding to one Em maximum (380 nm) and was similar to a microbial humic-like fluorophores (Kowalczuk et al., 2009; Osburn et al. 2011, 2012; Shutova et al., 2014). C4 had spectral characteristics (Ex: ≤ 230 and 270 nm/Em: 300 nm) similar to those of a tyrosine-like fluorophores (Murphy et al., 2011; Osburn et al., 2011). C5 (≤230(285)/340 nm) and C6 (275/324 nm) can both be characterised as tryptophan-like substances or tannin-like polyphenolic moieties (Hur et al., 2011), with C6 being slightly blue-shifted (Murphy et al., 2011; Kowalczuk et al., 2013). A recent study revealed that C4 and C6 are related closely to the low-molecular-weight organic acids acetate and butyrate (Drake et al., 2015).

3.2. Drivers of CH_4 ebullition

The mean CH_4 ebullition of the high nutrient and low nutrient treatments was 41.5 ± 52.3 mg CH_4–C m^{-2} d^{-1} and 3.6 ± 5.4 mg CH_4–C m^{-2} d^{-1}, respectively (Fig. 1). The mean ebullitive CH_4 flux was significantly higher in the high nutrient relative to the low nutrient treatments in all the ambient unheated groups (AMB), intermediate temperature groups (A2, +2–3 °C) and the warmest (A2+, +4–5 °C) temperature groups (*t*-test, $p < 0.001$; Fig. 1; Table S1). We found a significantly higher mean ebullitive CH_4 flux in the A2 and A2+ scenarios compared with the AMB scenario for the high nutrient group (*t*-test, $p < 0.05$; Fig. 1; Table S1), while no significant difference was found between A2 and A2+ for the high nutrient group (Fig. 1; Table S1). No significant difference was observed in mean ebullitive CH_4 flux among the three temperature treatments for the low nutrient group (ANOVA, Fig. 1; Table S1).

Elevated nutrient levels have shifted the mesocosms from a macrophyte-dominated clear water state to an algal-dominated turbid state, thereby changing the physico-chemical conditions of the water column (Liboriussen et al., 2005) (Fig. 1). Similar trends were found for Chl-*a*, DOC, BDOC, δ^{13}C-DOC, PARAFAC-components C1–C3 and C5–C6 with significantly higher mean values in the high nutrient than in the low nutrient treatments in all the AMB, A2 and A2+ temperature scenarios (*t*-test, $p < 0.001$; Fig. 1; Fig. S3; Table S1). We recorded a significantly higher mean F_{max} of C4 in the high compared with the low nutrient treatments in the A2 and A2+ groups (*t*-test, $p < 0.05$; Fig. 1; Fig. S3; Table S1), while no significant difference occurred in the AMB group. In comparison, mean macrophyte abundance (PVI) was notably lower in the high compared with the low nutrient group (*t*-test, $p < 0.001$; Fig. 1; Table S1). Note that the source water (groundwater) had a mean δ^{13}C-DOC of −27.2 ± 0.1‰, a typical value for terrestrial soil-derived DOM, and mean δ^{2}H and δ^{18}O were −55.9 ± 0.1‰ and −8.3 ± 0.3‰, respectively.

3.3. FT-ICR MS results

van Krevelen diagrams are graphical plots of atomic H/C ratios

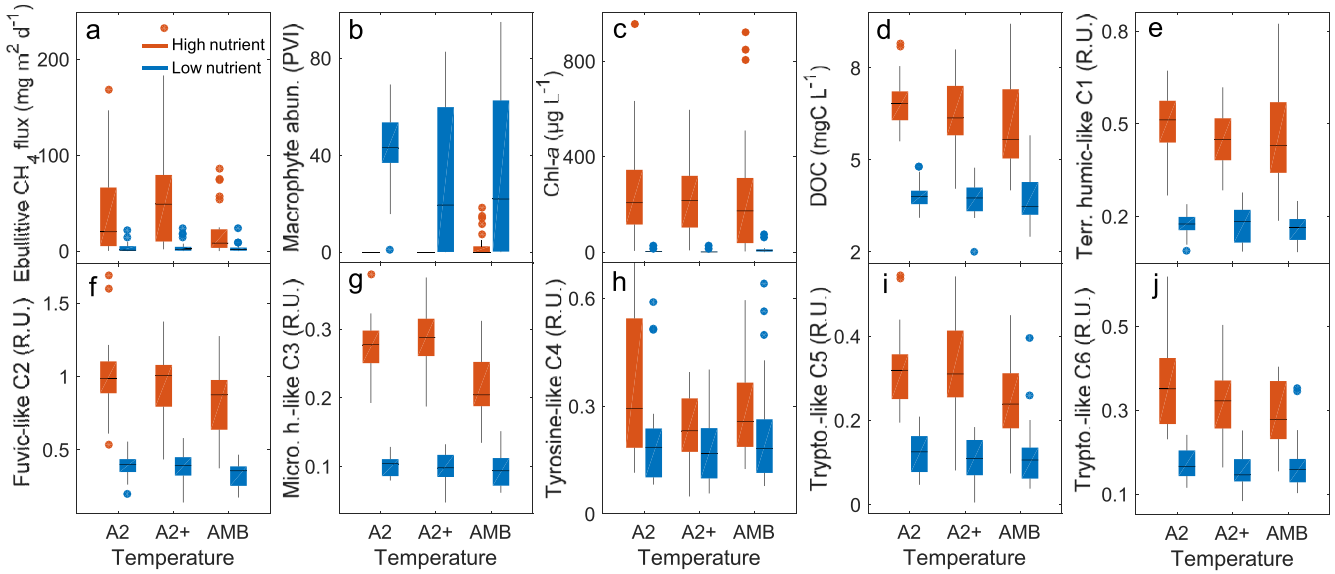

Fig. 1. Ebullitive CH4 flux (a), macrophyte abundance (PVI, b), chlorophyll-*a* (Chl-*a*, c), DOC (d), terrestrial humic-like C1 (e), fulvic-like C2 (f), microbial humic-like C3 (g), tyrosine-like C4 (h), and tryptophan-like C5–C6 (i–j) in samples collected from all mesocosms during the sampling period. AMB: Ambient temperature; A2 treatment: 2–4 °C higher than ambient; and A2+ treatment: 4–6 °C higher than ambient. Orange and blue boxes represent samples collected from high and low nutrient mesocosms, respectively. In all the six panels, boxes show medians, quartiles and extreme values. (For interpretation of the references to colour in this figure legend, the reader is referred to the Web version of this article.)

depicted against O/C ratios at molecular level and can be used to trace the sources and possible reaction pathways of DOM molecules in various aquatic environments (Kim et al., 2003; Dittmar and Paeng, 2009; Stubbins et al., 2010; Spencer et al., 2014; Kellerman et al., 2015). We selected samples collected from the AMB and A2 temperature scenarios crossed with the two nutrient levels to exhibit how eutrophication and warming may change the molecular signature of DOM (Fig. 2). For the AMB temperature scenario, a decreased relative abundance at molecular weight *m/z* 500–800 was recorded for the DOM sample collected from the high relative to the low nutrient treatment (Fig. 2). This resulted in an increased relative abundance of lipids, amino acids associated with proteins, and lignins, and a decreased relative abundance of carbohydrates and unsaturated hydrocarbons for the high relative to the low nutrient treatment (Fig. 2; Fig. S4). For the A2 scenario, in comparison, eutrophication decreased the average molecular weight of DOM collected from the high relative to the low nutrient treatment, resulting in a shifting of the bell-like relative intensity distribution centered from around *m/z* 400 to *m/z* 350 (Fig. 2). A notable higher relative abundance of lipids, amino acids associated with proteins were found for the high relative to the low nutrient mesocosms (Fig. 2; Fig. S4). For the AMB and A2 scenarios crossed with the two nutrient treatments, lipids and amino acids associated with proteins contributed 1530–2251 peaks (Zhou et al., 2018a), which represent 15.1%–30.9% of the total assigned formulas and 9.3%–34.5% of total relative abundance (Tables S2–S3). Aliphatic compounds contributed 1697–2562 peaks, making up a contribution of 17–41% of the total assigned formulas and 11.1%–49.5% of total relative abundance for the above mentioned four samples (Table S4). In comparison, lignins contributed 2392–8688 signals, represent 42%–70% of the total formulas assigned and 34.6%–71.6% of the total relative abundance of the four DOM samples (Fig. S4; Tables S2–S3). This constituted the greatest contribution percentages to the total assigned formulas, the results being consistent with those of a previous study in the same experimental facility, showing that terrestrial humic-rich fluorophores contributed significantly to the EEMs spectrum (Fig. S3) (Zhou et al., 2018a). Lipids, proteins and amino sugars often originate from microbial degradation of algal biomass in aquatic ecosystems, while lignin can be categorised as the unique remnants of terrestrial organic-rich DOM (Dittmar and Paeng, 2009; Stubbins et al., 2010; Spencer et al., 2014; Kellerman et al., 2015).

In this study, CHO contributed 2445–4653 peaks, accounting for 37%–43% of the total formulas assigned and 37.7%–45.2% of the total relative abundance to the AMB and A2 treatments crossed with low and high nutrients (Table S4). In comparison, CHON-only and CHOS-only compounds contributed 2544–5284 and 750–2666 peaks or 39%–44% and 13%–21% of the total assigned formulas, corresponding to 30.6%–53.0% and 9.2%–27.5% of the total relative abundance, respectively (Table S4).

A total of 3705 peaks were correlated notably with CH_4 ebullition with absolute Spearman rank correlation coefficients $|r| \geq 0.4$ (Fig. 2). We found the relative abundance of a total of 3031 peaks, mostly lipids, proteins, and lignins were positively correlated to CH_4 ebullition, while the remaining 674 peaks, mostly unsaturated hydrocarbons, negatively correlated to CH_4 ebullition (Fig. 2).

3.4. Relationships between macrophyte abundance, Chl-a, DOM-related indices and ebullitive CH_4 flux, and PCA results

We found that the ebullitive CH_4 flux was significantly negatively related to macrophyte abundance (PVI) and positively with algal Chl-*a* (Fig. 3). The ebullitive CH_4 flux was also significantly positively related to DOC, *a*(350), BDOC, δ^{13}C-DOC and F_{max} of all the six PARAFAC components (Fig. 3). Notably, the r^2 for the linear models between all the six components and the ebullitive CH_4 flux for the twenty-four mesocosms were higher than 0.4 (Fig. 3).

Eutrophication increased the concentration of autochthonous DOM and lowered the specific heat capacity in the water column of the high nutrient mesocosms, which resulted in enriched δ^2H and δ^{18}O. We found significant positive relationships between surface water δ^2H and ebullitive CH_4, δ^{13}C-DOC, DOC, fulvic-like C2, microbial humic-like C3 and tryptophan-like C5–C6 (Fig. S5).

The concentration of autochthonous DOM was closely linked to

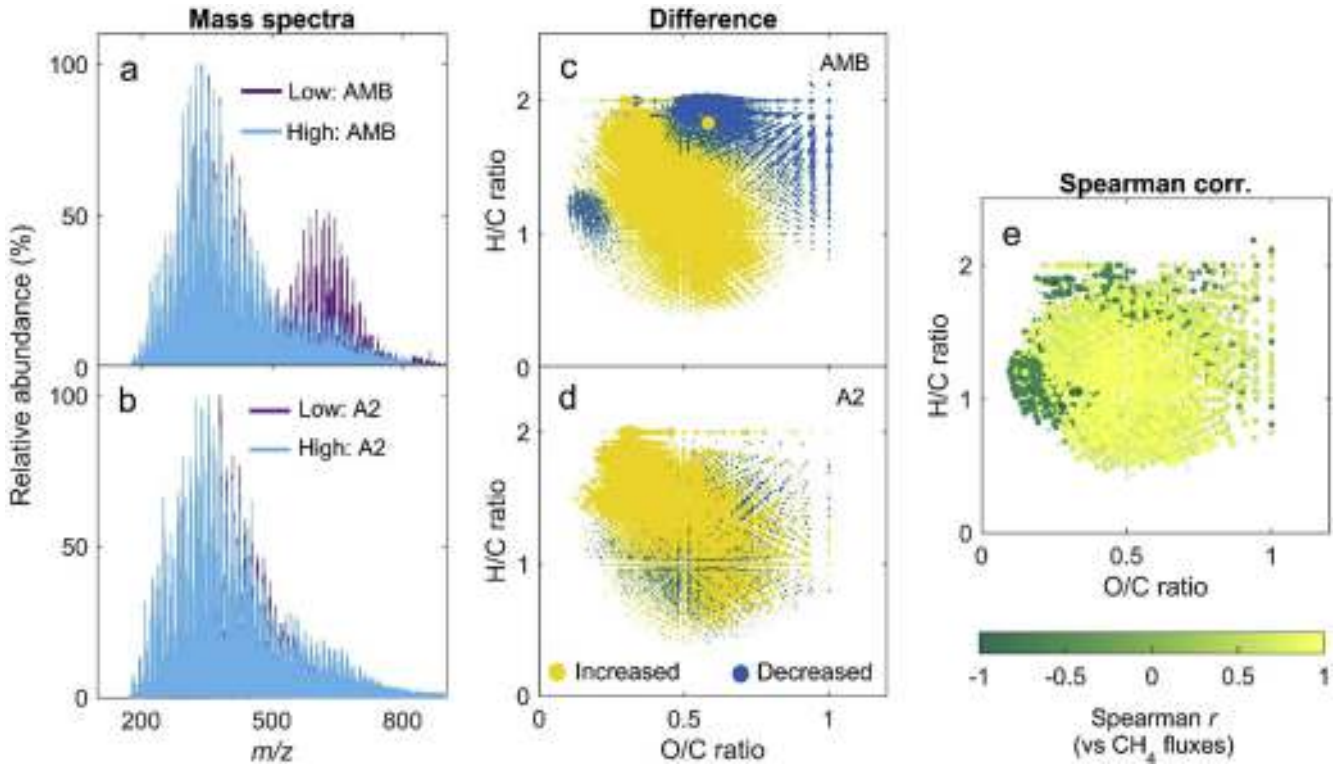

Fig. 2. Ultra-high resolution mass spectra (FT-ICR MS) over the *m/z* range 150–900 for the samples collected from collected from the low and high nutrient mesocosms associated with AMB and A2 scenarios (a–b). van Krevelen diagrams showing the O/C vs H/C ratio of all molecular formulae for the two samples with relative abundance increased or decreased for the high nutrient relative to the low nutrient treatments (c–d). The sizes of the dot are proportional to the changes in relative abundance of the FT-ICR MS identified molecules in panels c–d. Spearman correlation coefficients between relative abundances of FT-ICR MS identified molecules and mean ebullitive CH_4 fluxes from the corresponding mesocosms with $|r|>0.4$ shown only (e).

the algal blooms induced by nutrient addition. We found negative relationships between macrophyte abundance (PVI) and microbial humic-like C3, tyrosine-like C4 and tryptophan-like C5–C6 (Fig. 4). We further found positive relationships between algal Chl-*a* and C3–C6 (Fig. 4). These relationships indicate that degradation of algal Chl-*a* rather than macrophytes was the major source of autochthonous bio-labile DOM in the mesocosms. Enhanced accumulation of autochthonous bio-labile C3–C6 resulted in elevated BDOC of the DOM samples (Fig. 4). In one sample collected from low nutrient groups, the BDOC value (55%) was repeatedly identified as an outlier and this was therefore removed from the subsequent analyses (Fig. 3; Fig. 4).

We further used the *calc.relimp* function based on GLM modelling inbuilt in R to unveiling the relative importance of PVI, Chl-*a*, and DOM-related parameters in fueling CH_4 ebullition from the mesocosms. 77% of the variability of CH_4 ebullition was explained by a total of ten variables, including macrophyte abundance (PVI), Chl-*a*, DOC, *a*(350), PARAFAC-derived C1–C6 (Fig. 5). Among the ten variables, autochthonous bio-labile C3–C6 contributed to 46.5% of the variation explained (Fig. 5). Microbial humic-like C3 and tryptophan-like C5 were among the ten variables included in the *calc.relimp* with significance level $p < 0.01$ (Fig. 5). PCA can be used to produce a reduced dataset explaining the variation in the majority of variables, aiding in the interpretation of the variables with no prior knowledge (Bro and Smilde, 2014). In this study, we used PCA to summarizing the potential drivers of CH_4 ebullition and CH_4 efflux itself to unravel the potential linkage between CH_4 ebullition and autochthonous DOM. The interaction effects between each two of the variables used in PCA except for CH_4 efflux can be found in Table S5. In the PCA modeling of CH_4 ebullition, the PVI of submerged macrophytes, Chl-*a*, DOC, *a*(350), PARAFAC-derived C1–C6 during the experiment, no variable was stepwise excluded as the significant levels of the eleven indices were all < 0.001 (Table S6). The first two principal components, PC1 and PC2, explained 65.5% and 10.9%, respectively, of the total variability (Fig. 5). Log(CH_4), Chl-*a*, DOC, *a*(350) and PARAFAC-derived C1–C6 all displayed positive PC1 loading, while macrophyte PVI showed negative PC1 loading (Fig. 5). This result implies that PC1 was positively associated with the controls that fuel the outgassing of CH_4 ebullition, including algal biomass, DOC and algal-derived DOM. Tyrosine-like C4 displayed high PC2 loading (Fig. 5) an indication that PC2 was positively linked to the DOM remnant. Notably higher mean PC1 scores were found in the samples collected from the high than the low nutrient mesocosms in all temperature scenarios (*t*-test, $p < 0.001$; Fig. 5), while the effect of temperature on the PC1 scores was insignificant (Fig. 5).

3.5. 24 h bio-incubation results

The 24 h bio-incubation resulted in a rapid depletion of DOC and protein-like fluorophores and increasing dissolved CH_4 concentrations of both algal-DOM and soil-DOM samples (Fig. 6). After 24 h, dissolved CH_4 for algal-DOM and soil-DOM samples had increased from 12.5 ± 0.3 and 8.3 ± 0.1 nmol L^{-1} to 137.1 ± 4.3 and 18.9 ± 0.3 nmol L^{-1}, respectively (1001% and 128% increase, respectively, Fig. 6).

As for the algal-DOM samples, DOC decreased rapidly from 12.6 ± 0.5 to 2.7 ± 0.2 mg L^{-1} (a 78.4% decrease, Fig. 6). This was in coupled with a rapid decrease in fulvic-like C2, tyrosine-like C4, tryptophan-like C5 and C6 from 0.67 ± 0.04, 2.42 ± 0.13, 0.56 ± 0.01 and 2.42 ± 0.12 R.U. to 0.22 ± 0.02, 0.51 ± 0.07, 0.03 ± 0.03 and 0.68 ± 0.07 R.U., respectively (Fig. 6). We further found an increased

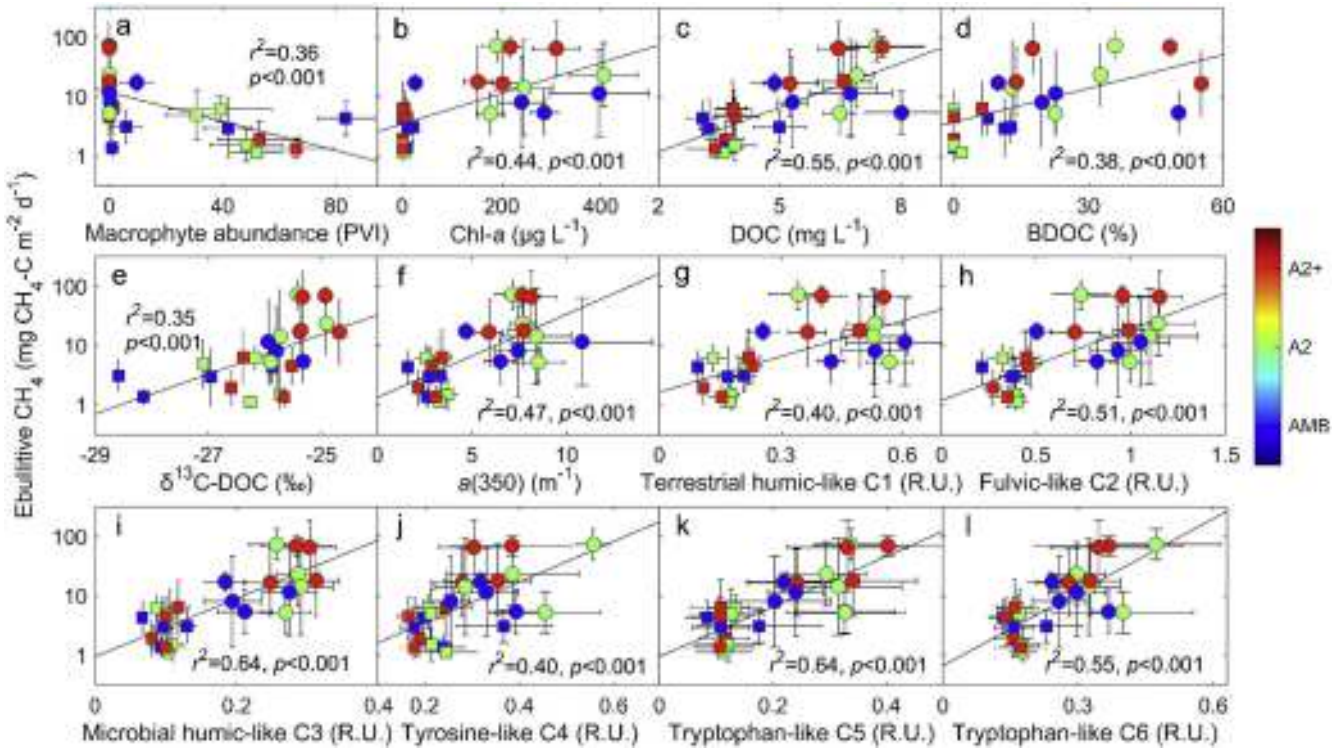

Fig. 3. Relationships between ebullitive CH_4 flux and macrophyte abundance (a), chlorophyll-*a* (Chl-*a*, b), dissolved organic carbon (DOC, c), bioavailable DOC (BDOC, d), stable isotopic δ^{13}C-DOC (e), CDOM absorption at 350 nm *a*(350) (f), terrestrial humic-like C1 (g), fulvic-like C2 (h). microbial humic-like C3 (i), tyrosine-like C4 (j) and tryptophan-like C5–C6 (k–l). Colours show different temperature scenarios, and squares and circles represent samples collected from low and high nutrient mesocosms, respectively. In all panels except for Chl-*a* (±1 standard errors, n = 16), error bars represent ± 1 S.D. of samples collected from each mesocosm during the experiment. (For interpretation of the references to colour in this figure legend, the reader is referred to the Web version of this article.)

F_{max} of terrestrial humic-like C1 and microbial humic-like C3 from 0.01 ± 0.01 and 0.05 ± 0.00 R.U. to 0.48 ± 0.05 and 0.22 ± 0.00 R.U., respectively (Fig. 6).

For soil-DOM, in comparison, DOC decreased from 15.3 ± 0.2 to 11.7 ± 0.3 mg L^{-1} (a 23.6% decrease, Fig. 6). C1–C4 and C6 decreased from 1.04 ± 0.01, 2.00 ± 0.01, 0.50 ± 0.00, 1.12 ± 0.05 and 1.61 ± 0.08 R.U. to 1.03 ± 0.08, 1.59 ± 0.16, 0.37 ± 0.02, 0.56 ± 0.04 and 0.78 ± 0.06 R.U., respectively (Fig. 6). We further found an increased F_{max} of C5 from 0.02 ± 0.03 to 0.12 ± 0.03 R.U. (Fig. 6).

4. Discussion

Our results indicate that CH_4 ebullition in shallow-lake mesocosms is shaped by a chain of eutrophication and temperature induced changes in ecosystem structure and function. This change is characterised by the shift in the balance between macrophyte abundance (PVI) and phytoplankton biomass (Chl-*a*), which in turn alters the accumulation of autochthonous bio-labile DOM. The temperature dependence of CH_4 production appears to play only a minor direct role compared with the other variables as increased temperature resulted in a weak but insignificant increase in ebullition during the June–August observation time (Fig. 1). This is not completely consistent with a previous study in the same experimental facility (Davidson et al., 2018), and the difference may stem from the different timescales covered by the studies, for example the lengthening the growing season, may be the reason for the more marked temperature effects found in studies covering an entire year (Davidson et al., 2018). Our PCA results suggested that eutrophication likely enhanced algal blooms and potentially contribute to the loss of submerged macrophytes (Fig. 5). The replacement of submerged macrophytes by dense algal biomass likely enhanced CH_4 ebullition (Fig. 3; Fig. 6), and is consistent with recent studies (Aben et al., 2017; Davidson et al., 2018). When the abundances of submerged macrophytes (PVI) were low and nutrient levels generally high, there remained a large degree of variation in ebullition. This may partially be explained by the variations in algal biomass, as was supported by the linkages among Chl-*a*, DOM composition, and CH_4 ebullition (Fig. 3; Fig. 4; Fig. 6). Other studies have shown that high algal biomass is associated with increased CH_4 ebullition (West et al., 2012; DelSontro et al., 2016). DOM derived from algal degradation can be highly bio-labile (Zhang et al., 2009; Zhou et al. 2015, 2018a) and this labile DOM fraction presumably leads to archaeal methanogenesis (Bogard et al., 2014; Repeta et al., 2016; Tang et al., 2016; Yao et al., 2016), possibly augmenting CH_4 ebullition also in the shallow-lake mesocosms (Fig. 5). Ebullition is in the end controlled by CH_4 production rates – when these exceed dissolution rates then bubbles are formed and it may be that highly labile DOM is key for these production rates to exceed this critical value.

The combination of our different experimental results suggest that microbial mineralization of autochthonous bio-labile DOM potentially increases CH_4 production to levels that far exceed the potential for dissolution likely resulting in enhanced CH_4 ebullition. The evidence of this is as follows: 1) Our 24 h bio-incubation experiment indicated that, compared with soil-DOM, autochthonous algal-DOM was highly bio-labile, with rapid depletion of DOC and autochthonous CDOM fluorophores (tyrosine-like C4 and tryptophan-like C5–C6), elevated bio-refractory terrestrial humic-like C1, coupled with a rapid increase of dissolved CH_4 (Fig. 6). As no sediment or particulate organic matter was added to the headspace bottles, markedly higher CH_4 outgassing from algal-DOM compared with soil-DOM bottles likely reflect archaea

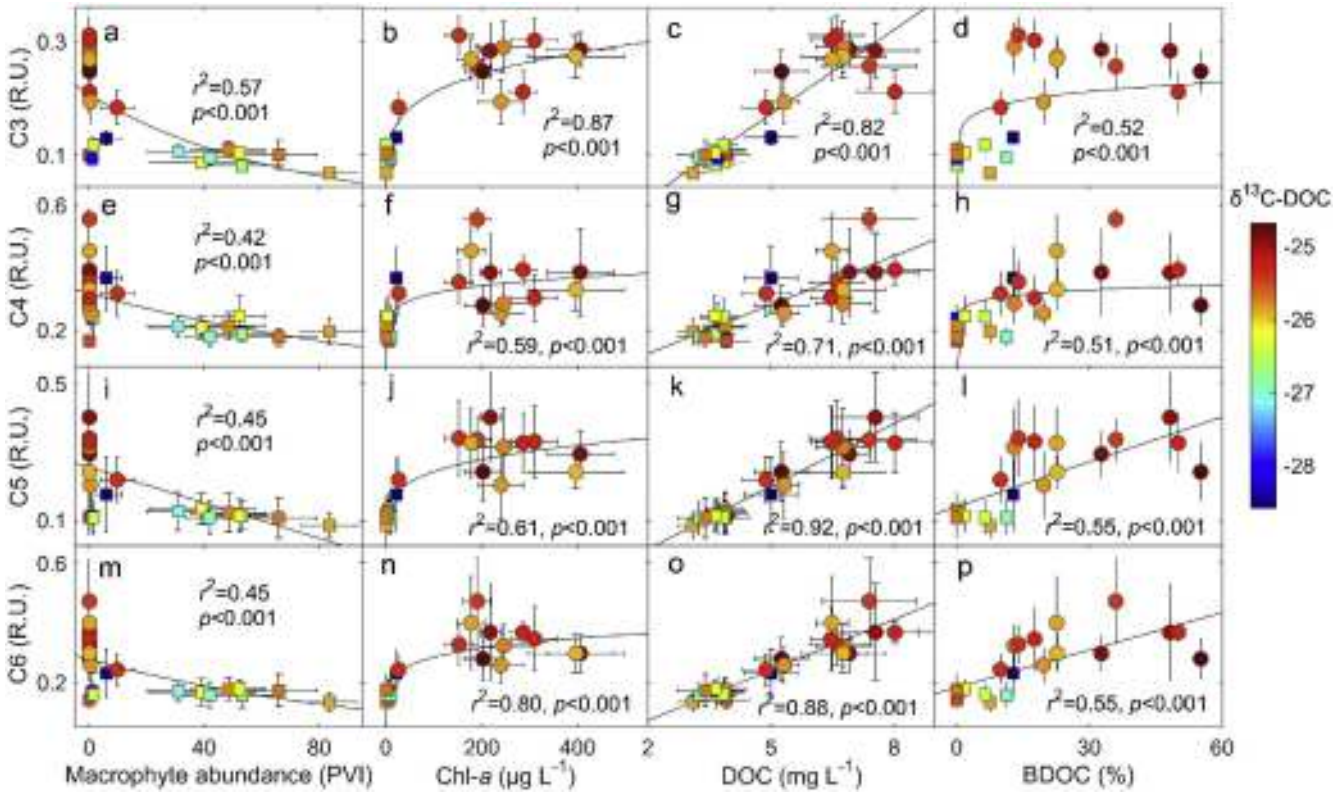

Fig. 4. Relationships between PARAFAC-derived autochthonous C3–C6 and macrophyte abundance (PVI), chlorophyll-*a* (Chl-*a*), dissolved organic carbon (DOC), and bioavailable DOC (BDOC) (a–p). In all panels, colour denotes stable isotopic δ^{13}C-DOC values (‰). Error bars in all panels represent ±1 S.D., except for Chl-*a* are the standard errors of samples collected from each mesocosm during the experiment. (For interpretation of the references to colour in this figure legend, the reader is referred to the Web version of this article.)

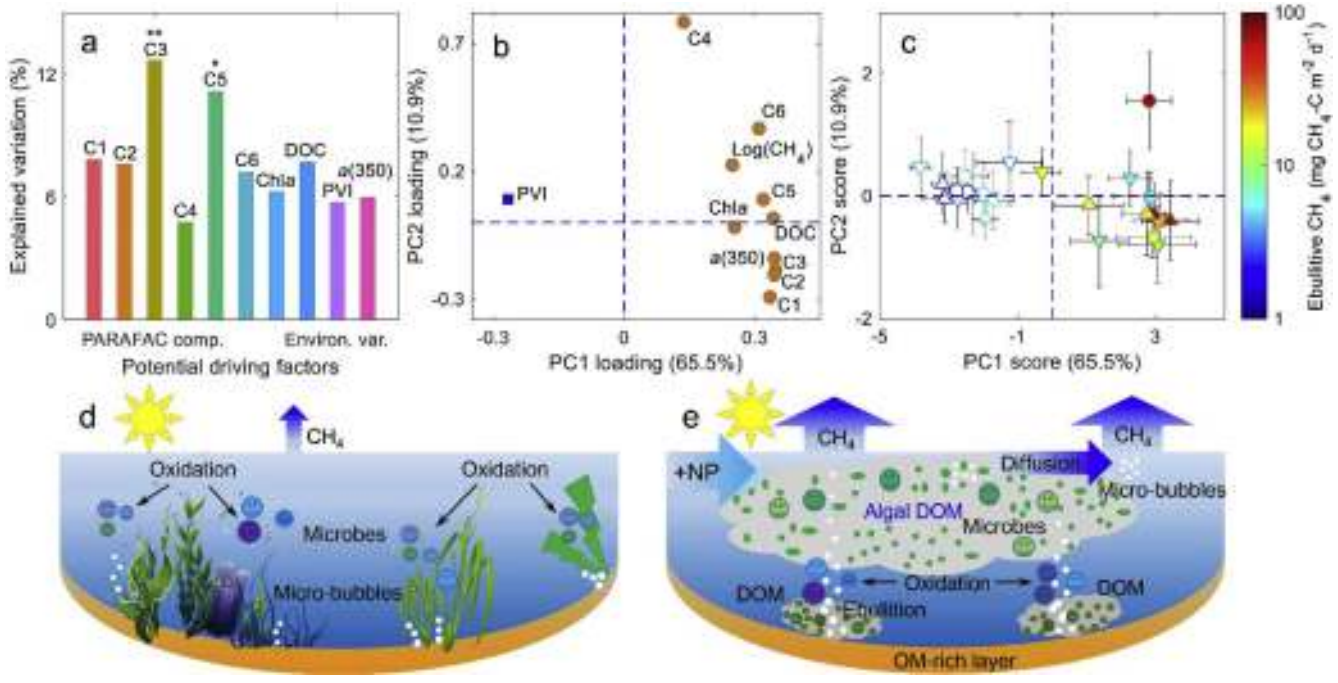

Fig. 5. The relative importance of individual variables, including the PVI of macrophytes, Chl-*a*, DOC, and CDOM optical properties to the ebullition of CH_4, i.e. the percentage of variation explained (a), **: $p < 0.005$; *: $p < 0.01$. PCA factor loadings (b) and scores (c) for the samples collected in the mesocosm experiment; hollow and closed dots in panel c represent samples collected from the low and high nutrient mesocosms, respectively, and ▽, ○, and △ stand for the samples collected in the AMB, A2, and A2+ temperature scenarios, respectively. The significant levels of the variables used in panel b were all <0.001. Error bars in panel c represent ±1 S.D. of samples collected from each mesocosm during the experiment. Conceptual diagram illustrating the multiple controls of the ebullitive CH_4 flux from the mesocosms without (d) and with (e) extra nutrient addition.

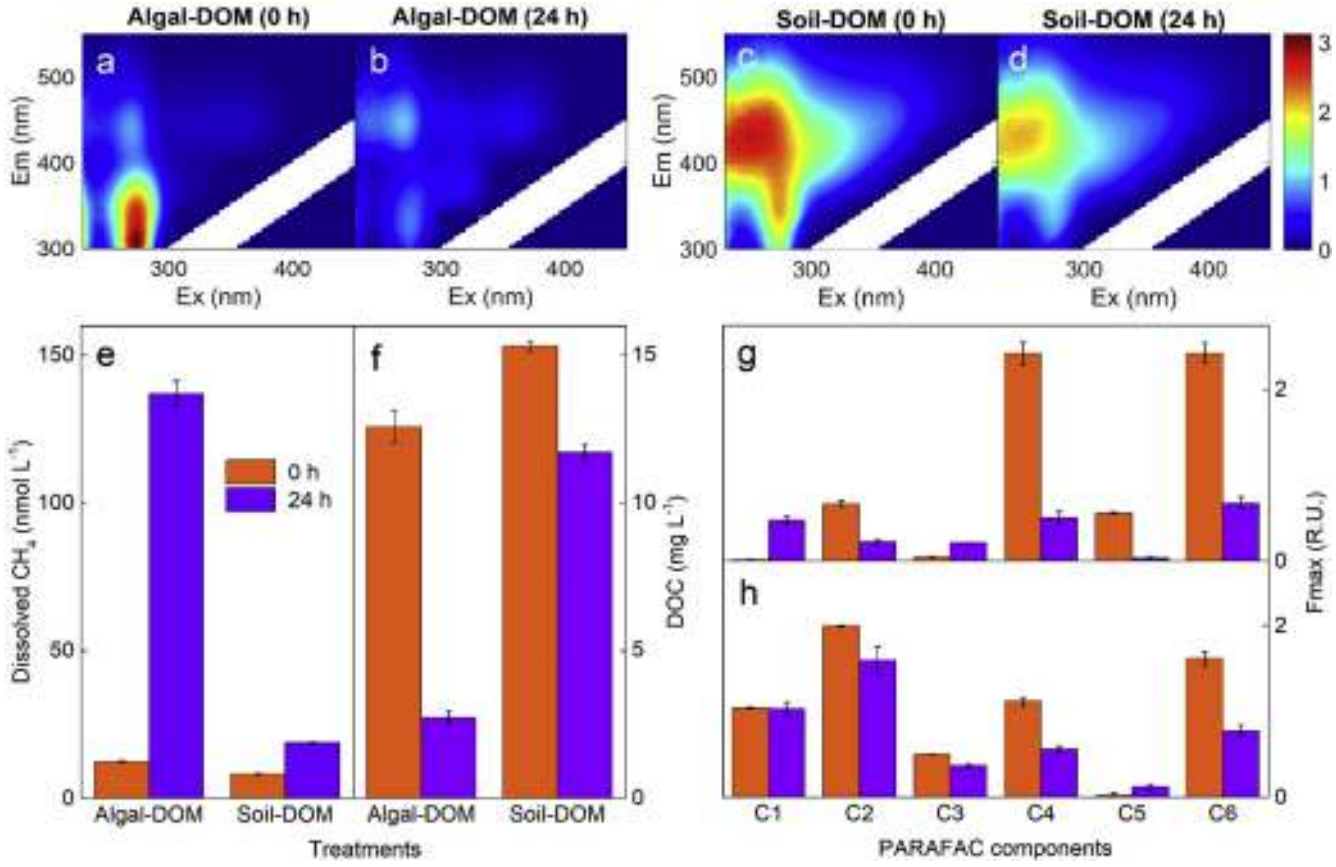

Fig. 6. Fluorescence signatures of algal-DOM and soil-DOM pre- and post-a 24 h bio-incubation (a–d). Fluorescence intensity shown in panels a–d are in Raman unit (R.U.). Variations of dissolved CH_4, DOC concentrations, and F_{max} of all six PARAFAC components for algal-DOM and soil-DOM pre- and post- 24 h bio-incubation (e–h). Error bars in panel e–h represent ±1 S.D. of triplicate samples.

cycling of the highly bio-labile autochthonous DOM (Fig. 6). This is consistent with a recent study that autochthonous tyrosine-like C3 and tryptophan-like C6 are closely linked with low-molecular-weight organic acids acetate and butyrate that can be rapidly consumed by microbial uptake (Drake et al., 2015). These results suggest that a rapid microbial reworking of autochthonous bio-labile DOM (within 24 h) likely fuelled the accumulation of high levels of CH_4 in the algal-DOM headspace bottles. 2) We found a notably higher CH_4 ebullition from the high compared with the low nutrient mesocosms across the different temperature scenarios, which was coincident with higher levels of autochthonous C3–C6 in the high relative to the low nutrient mesocosms (Fig. 1; Fig. 5; Table S1). Our conclusion is further supported by the positive relationships between the ebullitive CH_4 flux and δ^{13}C-DOC, δ^2H, and δ^{18}O (Fig. 3; Fig. S5). Enriched δ^{13}C-DOC, δ^2H and δ^{18}O levels were traced in the samples collected from the high but not from the low nutrient mesocosms (Table S1; Fig. S5) suggesting accumulation of autochthonous DOM in the mesocosms with high nutrient addition. Extra nutrient addition to the high nutrient mesocosms boosts planktonic algal biomass with higher Chl-*a* and autochthonous C3–C6 in these compared with the low nutrient mesocosms (Fig. 1; Fig. 5; Table S1). Numerous studies have shown that the microbial humic-like component (C3), tyrosine-like C4 and tryptophan-like fluorophores (C5–C6 in this study) are either produced from microbial mineralization of algal scums in eutrophic waters (Yamashita and Tanoue, 2004; Stedmon and Markager, 2005b; Zhang et al., 2009; Zhou et al., 2015) or residential sewage (Stedmon et al., 2011). The variability of these four autochthonous fluorescent components during the 8-week experimental observation period and the 24 h bio-incubation can therefore be regarded as a balance of fresh production and microbial degradation (Zhang et al., 2009). 3) The fractions of autochthonous DOM, C3–C6, in the high nutrient mesocosms are highly bio-labile, as documented by the positive relationships between the autochthonous fluorescent components (C3–C6) and Chl-*a* and BDOC (Fig. 4). Compared with PVI of macrophytes and Chl-*a*, the contribution percentage of autochthonous C3–C6 to the variation explained of CH_4 ebullition were notably higher (Fig. 5). This result was further supported by the increased contribution and also higher relative abundance of lipids and proteins identified using FT-ICR MS in the high relative to the low nutrient mesocosms (Fig. 2; Fig. S4). The positive Spearman rank correlations between CH_4 ebullition and the relative abundance of the lipids and proteins and also a fraction of lignins (Fig. 2) provided further evidence of this. Previous studies have suggested that the lipid and protein molecules can be highly bio-labile (Stubbins et al., 2012; Kellerman et al. 2015, 2018; Feng et al., 2016). The microbial cycling of these bio-labile fractions of DOM possibly increased the ebullition of CH_4 (Thauer et al., 2008; Bogard et al., 2014; Repeta et al., 2016) in the mesocosms as evidenced by the positive relationship between BDOC and CH_4 ebullition (Fig. 3). Archaea decomposition of bio-labile DOM associated with acetate and methylated compounds likely results in release of CH_4 as the end product (Murase and Sugimoto, 2005; Thauer et al., 2008; Bogard et al., 2014; Repeta et al., 2016; Tang et al., 2016) in the mesocosms with high nutrient addition.

It is not simple to quantify the relative importance of sediment organic matter and overlying DOM on CH_4 ebullition from the

experimental facility as dissolved oxygen consumption are prevailing near the bottom and also in the sediment, especially the high nutrient mesocosms (sediment being present in all the mesocosms). Also due to the shallow characteristics of the mesocosms with water depth approximately 1 m, the short residence time makes dissolution and oxidation unlikely to happen, contrary to what can be found in deep lakes (Beaulieu et al., 2016; Tang et al., 2016). Although changes in CH_4 ebullition cannot distinguish its carbon source from the sediment or the overlying water columns in the mesocosms, the combination of the mesocosm experiment and the 24 bio-incubation (Fig. 5; Fig. 6) exhibited the importance of autochthonous algal-DOM in enhancing ebullitive CH_4. In fluvial plain lakes and shallow lagoons with relatively long water residence time and excessive nutrient loadings from surrounding intensified urbanized areas, excessive algal blooms persist from early spring to late autumn or even the whole year (Qin et al., 2007; Ma et al., 2015). Extracellular polysaccharide substances and autochthonous DOM associated with the degradation of algal scums represent a large and highly bio-labile carbon pool, and their accumulation potentially enhance CH_4 effluxes from these environments (West et al. 2012, 2015; Xiao et al., 2017; Davidson et al., 2018). Follow-up studies could benefit from quantifying the relative importance of sediment organic-rich pore water DOM and overlying water DOM on ebullitive CH_4 efflux by including and excluding sediment in mesocosm experiments. The mesocosms are all fed by groundwater (Liboriussen et al., 2005), and the higher DOM concentration in the high nutrient compared with the low nutrient mesocosms must be derived from autochthonous degradation of algal biomass since the initial conditions were identical (Liboriussen et al., 2005; Zhou et al., 2018a). A recent study conducted in the same mesocosm facility have revealed that nutrient enrichment decreased the relative contribution of CH_4 diffusion from ~50% to merely 5%, and the diffusive flux (with mean efflux < 2 mg C m^{-2} d^{-1} in all mesocosms) exhibited no or limited response to eutrophication and warming (Davidson et al., 2018), and is therefore not discussed further here. Future research may also focus on quantifying the relative importance of allochthonous and autochthonous DOM from various environments in the outgassing of CH_4 by examination of methane isotopes and microbial communities.

5. Conclusions

This study is among the first to demonstrate the rapid depletion of bio-labile DOM potentially fuels the ebullition of CH_4 in high-nutrient mesocosms with high algal Chl-*a*. The changes of DOC, CDOM absorption and fluorescence, stable isotopes and ultrahigh-resolution mass spectrometry provides insight into the quantitative and compositional changes in the organic carbon pool during the experimental period and the 24 h bio-incubation. Eutrophication is among the most profound anthropogenic impacts on shallow lakes, the most abundant water body type worldwide, probably fueling the accumulation of autochthonous bio-labile DOM and the emission of CH_4 in these waters. Our results therefore strongly suggested that carbon cycling rate in shallow eutrophic waters might be significantly underestimated.

Author contributions

Y.Q.Z., L.Z., Y.L.Z., J.G.d.S., D.C.P., R.G.M.S., E.J., and T.A.D. conducted the research and performed the analyses. Y.Q.Z. wrote the manuscript with support from T.A.D., Y.L.Z., and E.J. All authors contributed to interpreting the results and discussions.

Declaration of competing interest

The authors declare that they have no known competing financial interests or personal relationships that could have appeared to influence the work reported in this paper.

Acknowledgments

This study was jointly funded by the National Natural Science Foundation of China (grants 41807362, 41621002, 41977322, and 41661134036), the Provincial Natural Science Foundation of Jiangsu in China (BK20181104), NIGLAS Cross-functional Innovation Teams (NIGLAS2016TD01) and NIGLAS Foundation (NIGLAS2017QD08). The facility where this work was carried out was supported by AQUACOSM (Network of Leading European AQUAtic MesoCOSM Facilities Connecting Mountains to Oceans from the Arctic to the Mediterranean) and PROGNOS (Predicting in-lake RespOnses to chanGe using Near real time MOdelS- Water joint programme initiative) and ANAEE (anaee.dk). E.J. and T.A.D. were further supported by Carlsberg Foundation. FT-ICR MS was partially supported by the NSF (DMR-1157490), the State of Florida and the FSU Future Fuels Institute. The authors thank all people in the NHMFL ICR Program who work selflessly to facilitate data acquisition and processing for users of the facility. We would like to express our deep thanks to Anne Mette Poulsen from Aarhus University for editorial assistance. We would also like to thank Yu Shi, Liuqing Zhang, Yuanpeng Li, Zhong Xia, Kirsten Landkildehus Thomsen and Chengying Zhang for their help with sampling and laboratory measurements. We thank the Editorial Board of Water Research and the three anonymous reviewers for their very constructive comments.

Appendix A. Supplementary data

Supplementary data to this article can be found online at https://doi.org/10.1016/j.watres.2019.115048.

References

Abbott, B.W., Larouche, J.R., Jones, J.B., Bowden, W.B., Balser, A.W., 2014. Elevated dissolved organic carbon biodegradability from thawing and collapsing permafrost. J. Geophys. Res.: Biogeosciences 119 (10), 2049–2063.

Aben, R.C.H., Barros, N., van Donk, E., Frenken, T., Hilt, S., Kazanjian, G., Lamers, L.P.M., Peeters, E., Roelofs, J.G.M., de Senerpont Domis, L.N., Stephan, S., Velthuis, M., Van de Waal, D.B., Wik, M., Thornton, B.F., Wilkinson, J., DelSontro, T., Kosten, S., 2017. Cross continental increase in methane ebullition under climate change. Nat. Commun. 8 (1), 1682.

Bastviken, D., Cole, J., Pace, M., Tranvik, L., 2004. Methane emissions from lakes: dependence of lake characteristics, two regional assessments, and a global estimate. Glob. Biogeochem. Cycles 18, GB4009.

Beaulieu, J.J., Mcmanus, M.G., Nietch, C.T., 2016. Estimates of reservoir methane emissions based on a spatially balanced probabilistic-survey. Limnol. Oceanogr. 61, S27–S40.

Bogard, M.J., del Giorgio, P.A., Boutet, L., Chaves, M.C., Prairie, Y.T., Merante, A., Derry, A.M., 2014. Oxic water column methanogenesis as a major component of aquatic CH4 fluxes. Nat. Commun. 5, 5350.

Borges, A.V., Darchambeau, F., Teodoru, C.R., Marwick, T.R., Tamooh, F., Geeraert, N., Omengo, F.O., Guérin, F., Lambert, T., Morana, C., Okuku, E., Bouillon, S., 2015. Globally significant greenhouse-gas emissions from African inland waters. Nat. Geosci. 8 (8), 637–642.

Bro, R., Smilde, A.K., 2014. Principal component analysis. Anal. Meth. 6 (9), 2812–2831.

Ciais, P., Sabine, C., Bala, G., Bopp, L., Brovkin, V., Al, E., House, J.I., 2014. Carbon and other biogeochemical cycles. In: Climate Change 2013: the Physical Science Basis. Cambridge University Press, pp. 465–570.

Coble, P.G., 2007. Marine optical biogeochemistry: the chemistry of ocean color. Chem. Rev. 107, 402–418.

Davidson, T.A., Audet, J., Jeppesen, E., Landkildehus, F., Lauridsen, T.L., Søndergaard, M., Syväranta, J., 2018. Synergy between nutrients and warming enhances methane ebullition from experimental lakes. Nat. Clim. Chang. 8, 156–160.

Davidson, T.A., Audet, J., Svenning, J.C., Lauridsen, T.L., Sondergaard, M., Landkildehus, F., Larsen, S.E., Jeppesen, E., 2015. Eutrophication effects on

greenhouse gas fluxes from shallow-lake mesocosms override those of climate warming. Glob. Chang. Biol. 21 (12), 4449–4463.
DelSontro, T., Beaulieu, J.J., Downing, J.A., 2018a. Greenhouse gas emissions from lakes and impoundments: upscaling in the face of global change. Limnol. Oceanogr. Lett. 3, 64–75.
DelSontro, T., Boutet, L., St-Pierre, A., Del Giorgio, P.A., Prairie, Y.T., 2016. Methane ebullition and diffusion from northern ponds and lakes regulated by the interaction between temperature and system productivity. Limnol. Oceanogr. 61, S62–S77.
DelSontro, T., Giorgio, P.A.D., Prairie, Y.T., 2018b. No longer a paradox: the interaction between physical transport and biological processes explains the spatial distribution of surface water methane within and across lakes. Ecosystems 21 (6), 1073–1087.
Dittmar, T., Koch, B., Hertkorn, N., Kattner, G., 2008. A simple and efficient method for the solid-phase extraction of dissolved organic matter (SPE-DOM) from seawater. Limnol Oceanogr. Methods 6, 230–235.
Dittmar, T., Paeng, J., 2009. A heat-induced molecular signature in marine dissolved organic matter. Nat. Geosci. 2 (3), 175–179.
Drake, T.W., Wickland, K.P., Spencer, R.G., McKnight, D.M., Striegl, R.G., 2015. Ancient low-molecular-weight organic acids in permafrost fuel rapid carbon dioxide production upon thaw. Proc. Natl. Acad. Sci. U.S.A. 112 (45), 13946–13951.
Feng, L., Xu, J., Kang, S., Li, X., Li, Y., Jiang, B., Shi, Q., 2016. Chemical composition of microbe-derived dissolved organic matter in cryoconite in Tibetan Plateau glaciers: insights from Fourier transform ion cyclotron resonance mass spectrometry analysis. Environ. Sci. Technol. 50 (24), 13215–13223.
Fu, Q., He, J., Blaney, L., Zhou, D., 2016. Roxarsone binding to soil-derived dissolved organic matter: insights from multi-spectroscopic techniques. Chemosphere 155, 225–233.
Guo, W., Yang, L., Zhai, W., Chen, W., Osburn, C.L., Huang, X., Li, Y., 2014. Runoff-mediated seasonal oscillation in the dynamics of dissolved organic matter in different branches of a large bifurcated estuary-The Changjiang Estuary. J. Geophys. Res.: Biogeosciences 119 (5), 776–793.
Hawkes, J.A., Hansen, C.T., Goldhammer, T., Bach, W., Dittmar, T., 2016. Molecular alteration of marine dissolved organic matter under experimental hydrothermal conditions. Geochem. Cosmochim. Acta 175, 68–85.
He, W., Hur, J., 2015. Conservative behavior of fluorescence EEM-PARAFAC components in resin fractionation processes and its applicability for characterizing dissolved organic matter. Water Res. 83, 217–226.
Holgerson, M.A., Raymond, P.A., 2016. Large contribution to inland water CO2 and CH4 emissions from very small ponds. Nat. Geosci. 9 (3), 222–226.
Holmes, R.M., McClelland, J.W., Raymond, P.A., Frazer, B.B., Peterson, B.J., Stieglitz, M., 2008. Lability of DOC transported by alaskan rivers to the arctic ocean. Geophys. Res. Lett. 35 (3), L03402.
Hood, E., Fellman, J., Spencer, R.G., Hernes, P.J., Edwards, R., D'Amore, D., Scott, D., 2009. Glaciers as a source of ancient and labile organic matter to the marine environment. Nature 462 (7276), 1044–1047.
Houghton, J.T., Ding, Y., Griggs, D.J., Noguer, M., van Der Linden, P.J., Dai, X., Maskell, K., Johnson, C.A., 2001. Climate Change 2001: the Scientific Basis. Contribution of Working Group I to the Third Assessment Report of the Intergovernmental Panel on Climate Change. Cambridge University Press, Cambridge.
Huang, C., Zhang, L., Li, Y., Lin, C., Huang, T., Zhang, M., Zhu, A.x., Yang, H., Wang, X., 2018. Carbon and nitrogen burial in a plateau lake during eutrophication and phytoplankton blooms. Sci. Total Environ. 616–617, 296–304.
Hur, J., Jung, K.Y., Schlautman, M.A., 2011. Altering the characteristics of a leaf litter-derived humic substance by adsorptive fractionation versus simulated solar irradiation. Water Res. 45 (18), 6217–6226.
Hur, J., Lee, B.-M., Lee, S., Shin, J.-K., 2014. Characterization of chromophoric dissolved organic matter and trihalomethane formation potential in a recently constructed reservoir and the surrounding areas – impoundment effects. J. Hydrol. 515, 71–80.
Hur, J., Park, M.-H., Schlautman, M.A., 2009. Microbial transformation of dissolved leaf litter organic matter and its effects on selected organic matter operational descriptors. Environ. Sci. Technol. 43 (7), 2315–2321.
Kellerman, A.M., Guillemette, F., Podgorski, D.C., Aiken, G.R., Butler, K.D., Spencer, R.G.M., 2018. Unifying concepts linking dissolved organic matter composition to persistence in aquatic ecosystems. Environ. Sci. Technol. 52 (5), 2538–2548.
Kellerman, A.M., Kothawala, D.N., Dittmar, T., Tranvik, L.J., 2015. Persistence of dissolved organic matter in lakes related to its molecular characteristics. Nat. Geosci. 8 (6), 454–457.
Kim, S., Kramer, R.W., Hatcher, P.G., 2003. Graphical method for analysis of ultrahigh-resolution broadband mass spectra of natural organic matter, the van Krevelen diagram. Anal. Chem. 75 (20), 5336–5344.
Kothawala, D.N., Stedmon, C.A., Muller, R.A., Weyhenmeyer, G.A., Kohler, S.J., Tranvik, L.J., 2014. Controls of dissolved organic matter quality: evidence from a large-scale boreal lake survey. Glob. Chang. Biol. 20 (4), 1101–1114.
Kowalczuk, P., Durako, M.J., Young, H., Kahn, A.E., Cooper, W.J., Gonsior, M., 2009. Characterization of dissolved organic matter fluorescence in the South Atlantic Bight with use of PARAFAC model: interannual variability. Mar. Chem. 113 (3–4), 182–196.
Kowalczuk, P., Tilstone, G.H., Zablocka, M., Röttgers, R., Thomas, R., 2013. Composition of dissolved organic matter along an Atlantic Meridional Transect from fluorescence spectroscopy and parallel factor analysis. Mar. Chem. 157, 170–184.
Liboriussen, L., Landkildehus, F., Meerhoff, M., Bramm, M.E., Søndergaard, M., Christoffersen, K., Richardson, K., Søndergaard, M., Lauridsen, T.L., Jeppesen, E., 2005. Global warming: design of a flow-through shallow lake mesocosm climate experiment. Limnol Oceanogr. Methods 3 (1), 1–9.
Ma, J., Qin, B., Paerl, H.W., Brookes, J.D., Hall, N.S., Shi, K., Zhou, Y., Guo, J., Li, Z., Xu, H., Wu, T., Long, S., 2015. The persistence of cyanobacterial (Microcystisspp.) blooms throughout winter in Lake Taihu, China. Limnol. Oceanogr. 61 (2), 711–722.
Mann, P.J., Davydova, A., Zimov, N., Spencer, R.G.M., Davydov, S., Bulygina, E., Zimov, S., Holmes, R.M., 2012. Controls on the composition and lability of dissolved organic matter in Siberia's Kolyma River basin. J. Geophys. Res.: Biogeosciences 117, G01028.
Mopper, K., Stubbins, A., Ritchie, J.D., Bialk, H.M., Hatcher, P.G., 2007. Advanced instrumental approaches for characterization of marine dissolved organic matter: extraction techniques, mass spectrometry, and nuclear magnetic resonance spectroscopy. Chem. Rev. 107 (2), 419–442.
Murase, J., Sugimoto, A., 2005. Inhibitory effect of light on methane oxidation in the pelagic water column of a mesotrophic lake (Lake Biwa, Japan). Limnol. Oceanogr. 50 (4), 1339–1343.
Murphy, K.R., Hambly, A., Singh, S., Henderson, R.K., Baker, A., Stuetz, R., Khan, S.J., 2011. Organic matter fluorescence in municipal water recycling schemes: toward a unified PARAFAC model. Environ. Sci. Technol. 45 (7), 2909–2916.
Murphy, K.R., Stedmon, C.A., Graeber, D., Bro, R., 2013. Fluorescence spectroscopy and multi-way techniques. PARAFAC. Analytical Methods 5 (23), 6557–6566.
Murphy, K.R., Stedmon, C.A., Waite, T.D., Ruiz, G.M., 2008. Distinguishing between terrestrial and autochthonous organic matter sources in marine environments using fluorescence spectroscopy. Mar. Chem. 108 (1–2), 40–58.
Murphy, K.R., Stedmon, C.A., Wenig, P., Bro, R., 2014. OpenFluor–an online spectral library of auto-fluorescence by organic compounds in the environment. Analytical Methods 6 (3), 658–661.
Ohno, T., Parr, T.B., Gruselle, M.C., Fernandez, I.J., Sleighter, R.L., Hatcher, P.G., 2014. Molecular composition and biodegradability of soil organic matter: a case study comparing two new England forest types. Environ. Sci. Technol. 48 (13), 7229–7236.
Osburn, C.L., Handsel, L.T., Mikan, M.P., Paerl, H.W., Montgomery, M.T., 2012. Fluorescence tracking of dissolved and particulate organic matter quality in a river-dominated estuary. Environ. Sci. Technol. 46 (16), 8628–8636.
Osburn, C.L., Wigdahl, C.R., Fritz, S.C., Saros, J.E., 2011. Dissolved organic matter composition and photoreactivity in prairie lakes of the U.S. Great Plains. Limnol. Oceanogr. 56 (6), 2371–2390.
Qin, B., Xu, P., Wu, Q., Luo, L., Zhang, Y., 2007. Environmental issues of Lake Taihu, China. Hydrobiologia 581 (1), 3–14.
Repeta, D.J., Ferrón, S., Sosa, O.A., Johnson, C.G., Repeta, L.D., Acker, M., DeLong, E.F., Karl, D.M., 2016. Marine methane paradox explained by bacterial degradation of dissolved organic matter. Nat. Geosci. 9 (12), 884–887.
Samad, M.S., Bertilsson, S., 2017. Seasonal variation in abundance and diversity of bacterial methanotrophs in five temperate Lakes. Front. Microbiol. 8 (142), 142.
Saunois, M., Bousquet, P., Poulter, B., Peregon, A., Ciais, P., Canadell, J.G., Dlugokencky, E.J., Etiope, G., Bastviken, D., Houweling, S., 2016. The global methane budget 2000–2012. Earth Syst. Sci. Data 8 (2), 697–751.
Shutova, Y., Baker, A., Bridgeman, J., Henderson, R.K., 2014. Spectroscopic characterisation of dissolved organic matter changes in drinking water treatment: from PARAFAC analysis to online monitoring wavelengths. Water Res. 54, 159–169.
Song, K., Shang, Y., Wen, Z., Jacinthe, P.A., Liu, G., Lyu, L., Fang, C., 2018. Characterization of CDOM in saline and freshwater lakes across China using spectroscopic analysis. Water Res. 150, 403–417.
Spencer, R.G.M., Guo, W., Raymond, P.A., Dittmar, T., Hood, E., Fellman, J., Stubbins, A., 2014. Source and biolability of ancient dissolved organic matter in glacier and lake ecosystems on the Tibetan Plateau. Geochem. Cosmochim. Acta 142, 64–74.
Spencer, R.G.M., Mann, P.J., Dittmar, T., Eglinton, T.I., McIntyre, C., Holmes, R.M., Zimov, N., Stubbins, A., 2015. Detecting the signature of permafrost thaw in Arctic rivers. Geophys. Res. Lett. 42, 2830–2835.
Stedmon, C.A., Bro, R., 2008. Characterizing dissolved organic matter fluorescence with parallel factor analysis: a tutorial. Limnol Oceanogr. Methods 6, 572–579.
Stedmon, C.A., Granskog, M., Dodd, P.A., 2015. An approach to estimate the freshwater contribution from glacial melt and precipitation in East Greenland shelf waters using colored dissolved organic matter (CDOM). J. Geophys. Res.: Oceans 120, 1107–1117.
Stedmon, C.A., Markager, S., 2005a. Resolving the variability in dissolved organic matter fluorescence in a temperate estuary and its catchment using PARAFAC analysis. Limnol. Oceanogr. 50 (2), 686–697.
Stedmon, C.A., Markager, S., 2005b. Tracing the production and degradation of autochthonous fractions of dissolved organic matter by fluorescence analysis. Limnol. Oceanogr. 50 (5), 1415–1426.
Stedmon, C.A., Markager, S., Bro, R., 2003. Tracing dissolved organic matter in aquatic environments using a new approach to fluorescence spectroscopy. Mar. Chem. 82 (3–4), 239–254.
Stedmon, C.A., Seredynska-Sobecka, B., Boe-Hansen, R., Le Tallec, N., Waul, C.K., Arvin, E., 2011. A potential approach for monitoring drinking water quality from groundwater systems using organic matter fluorescence as an early warning for contamination events. Water Res. 45 (18), 6030–6038.
Stedmon, C.A., Thomas, D.N., Granskog, M., Kaartokallio, H., Papadimitriou, S., Kuosa, H., 2007. Characteristics of dissolved organic matter in Baltic coastal sea

ice: allochthonous or autochthonous origins? Environ. Sci. Technol. 41 (21), 7273–7279.
Stubbins, A., Hood, E., Raymond, P.A., Aiken, G.R., Sleighter, R.L., Hernes, P.J., Butman, D., Hatcher, P.G., Striegl, R.G., Schuster, P., Abdulla, H.A.N., Vermilyea, A.W., Scott, D.T., Spencer, R.G.M., 2012. Anthropogenic aerosols as a source of ancient dissolved organic matter in glaciers. Nat. Geosci. 5, 198–201.
Stubbins, A., Spencer, R.G.M., Chen, H., Hatcher, P.G., Mopper, K., Hernes, P.J., Mwamba, V.L., Mangangu, A.M., Wabakanghanzi, J.N., Six, J., 2010. Illuminated darkness: molecular signatures of Congo River dissolved organic matter and its photochemical alteration as revealed by ultrahigh precision mass spectrometry. Limnol. Oceanogr. 55 (4), 1467–1477.
Tang, K.W., Mcginnis, D.F., Ionescu, D., Grossart, H.P., 2016. Methane production in oxic lake waters potentially increases aquatic methane flux to air. Environ. Sci. Technol. Lett. 3 (6), 227–233.
Tang, X., Chao, J., Gong, Y., Wang, Y., Wilhelm, S.W., Gao, G., 2017. Spatiotemporal dynamics of bacterial community composition in large shallow eutrophic Lake Taihu: high overlap between free-living and particle-attached assemblages. Limnol. Oceanogr. 62 (4), 1366–1382.
Thauer, R., Kaster, A., Seedorf, H.,W., Hedderich, R., 2008. Methanogenic archaea: ecologically relevant differences in energy conservation. Nat. Rev. Microbiol. 6 (8), 579–591.
Verpoorter, C., Kutser, T., Seekell, D.A., Tranvik, L.J., 2015. A global inventory of lakes based on high-resolution satellite imagery. Geophys. Res. Lett. 41 (18), 6396–6402.
Vonk, J.E., Tank, S.E., Mann, P.J., Spencer, R.G.M., Treat, C.C., Striegl, R.G., Abbott, B.W., Wickland, K.P., 2015. Biodegradability of dissolved organic carbon in permafrost soils and aquatic systems: a meta-analysis. Biogeosciences 12 (23), 6915–6930.
West, W.E., Coloso, J.J., Jones, S.E., 2012. Effects of algal and terrestrial carbon on methane production rates and methanogen community structure in a temperate lake sediment. Freshw. Biol. 57 (5), 949–955.
West, W.E., Mccarthy, S.M., Jones, S.E., 2015. Phytoplankton lipid content influences freshwater lake methanogenesis. Freshw. Biol. 60 (11), 2261–2269.
Wik, M., Crill, P.M., Varner, R.K., Bastviken, D., 2013. Multiyear measurements of ebullitive methane flux from three subarctic lakes. J. Geophys. Res. Biogeosci. 118 (3), 1307–1321.
Wik, M., Varner, R.K., Anthony, K.W., MacIntyre, S., Bastviken, D., 2016. Climate-sensitive northern lakes and ponds are critical components of methane release. Nat. Geosci. 9 (2), 99–105.
Xiao, Q., Zhang, M., Hu, Z., Gao, Y., Hu, C., Liu, C., Liu, S., Zhang, Z., Zhao, J., Xiao, W., Lee, X., 2017. Spatial variations of methane emission in a large shallow eutrophic lake in subtropical climate. J. Geophys. Res.: Biogeosciences 122 (7), 1597–1614.
Yamamoto-Kawai, M., 2005. Freshwater and brine behaviors in the Arctic Ocean deduced from historical data of δ18O and alkalinity (1929–2002 A.D.). J. Geophys. Res. 110, C10003.
Yamashita, Y., Tanoue, E., 2004. In situ production of chromophoric dissolved organic matter in coastal environments. Geophys. Res. Lett. 31 (14), L14302.
Yang, L., Zhuang, W.E., Chen, C.A., Wang, B.J., Kuo, F.W., 2017. Unveiling the transformation and bioavailability of dissolved organic matter in contrasting hydrothermal vents using fluorescence EEM-PARAFAC. Water Res. 111, 195–203.
Yao, M., Henny, C., Maresca, J.A., 2016. Freshwater bacteria release methane as a byproduct of phosphorus acquisition. Appl. Environ. Microbiol. 82 (23), 6994–7003.
Yao, X., Zhang, Y., Zhu, G., Qin, B., Feng, L., Cai, L., Gao, G., 2011. Resolving the variability of CDOM fluorescence to differentiate the sources and fate of DOM in Lake Taihu and its tributaries. Chemosphere 82 (2), 145–155.
Zhang, Y., van Dijk, M.A., Liu, M., Zhu, G., Qin, B., 2009. The contribution of phytoplankton degradation to chromophoric dissolved organic matter (CDOM) in eutrophic shallow lakes: field and experimental evidence. Water Res. 43 (18), 4685–4697.
Zhou, Y., Davidson, T.A., Yao, X., Zhang, Y., Jeppesen, E., de Souza, J.G., Wu, H., Shi, K., Qin, B., 2018a. How autochthonous dissolved organic matter responds to eutrophication and climate warming: evidence from a cross-continental data analysis and experiments. Earth Sci. Rev. 185, 928–937.
Zhou, Y., Jeppesen, E., Zhang, Y., Niu, C., Shi, K., Liu, X., Zhu, G., Qin, B., 2015. Chromophoric dissolved organic matter of black waters in a highly eutrophic Chinese lake: freshly produced from algal scums? J. Hazard Mater. 299, 222–230.
Zhou, Y., Xiao, Q., Yao, X., Zhang, Y., Zhang, M., Shi, K., Lee, X., Podgorski, D.C., Qin, B., Spencer, R.G.M., Jeppesen, E., 2018b. Accumulation of terrestrial dissolved organic matter potentially enhances dissolved methane levels in eutrophic Lake Taihu, China. Environ. Sci. Technol. 52, 10297–10306.